

Monte Carlo study of correction factors for Spencer–Attix cavity theory at photon energies at or above 100 keV

Jette Borg, Iwan Kawrakow, D. W. O. Rogers,^{a)} and Jan P. Seuntjens
Ionizing Radiation Standards, National Research Council of Canada, Ottawa K1A 0R6, Canada

(Received 24 August 1999; accepted for publication 22 May 2000)

To develop a primary standard for ^{192}Ir sources, the basic science on which this standard is based, i.e., Spencer–Attix cavity theory, must be established. In the present study Monte Carlo techniques are used to investigate the accuracy of this cavity theory for photons in the energy range from 20 to 1300 keV, since it is usually not applied at energies below that of ^{137}Cs . Ma and Nahum [Phys. Med. Biol. **36**, 413–428 (1991)] found that in low-energy photon beams the contribution from electrons caused by photons interacting in the cavity is substantial. For the average energy of the ^{192}Ir spectrum they found a departure from Bragg–Gray conditions of up to 3% caused by photon interactions in the cavity. When Monte Carlo is used to calculate the response of a graphite ion chamber to an encapsulated ^{192}Ir source it is found that it differs by less than 0.3% from the value predicted by Spencer–Attix cavity theory. Based on these Monte Carlo calculations, for cavities in graphite it is concluded that the Spencer–Attix cavity theory with $\Delta = 10$ keV is applicable within 0.5% for photon energies at 300 keV or above despite the breakdown of the assumption that there is no interaction of photons within the cavity. This means that it is possible to use a graphite ion chamber and Spencer–Attix cavity theory to calibrate an ^{192}Ir source. It is also found that the use of Δ related to the mean chord length instead of $\Delta = 10$ keV improves the agreement with Spencer–Attix cavity theory at ^{60}Co from 0.2% to within 0.1% of unity. This is at the level of accuracy of which the Monte Carlo code EGSnrc calculates ion chamber responses. In addition, it is shown that the effects of other materials, e.g., insulators and holders, have a substantial effect on the ion chamber response and should be included in the correction factors for a primary standard of air kerma. [S0094-2405(00)02008-3]

Key words: cavity theory, Monte Carlo EGSnrc, stopping-power ratio, ^{192}Ir , ion chamber

I. INTRODUCTION

For low-energy photons, primary standards of air kerma are usually based on free-air chambers in which a direct measure is made of the charge released in the air. These standards can not normally be applied above about 300 keV because the range of the electrons generated by the electrons becomes too long.¹ For higher-energy photons such as from ^{60}Co and ^{137}Cs sources (1250 and 662 keV average energies for bare sources), it is common to base primary standards of air kerma on the use of graphite-walled cavity ion chambers and the Spencer–Attix schematization of Bragg–Gray cavity theory.^{2,3} In the past, the National Institute for Standards and Technology (NIST) developed a primary standard for ^{192}Ir sources based on this approach.⁴ However, ^{192}Ir sources have a wide spectrum of photon energies, from less than 100 up to about 900 keV with an average energy, and the strongest photon intensities being at slightly over 300 keV.^{5,6} Ma and Nahum⁷ showed that at lower photon energies, a large fraction of the dose to the gas in an ion chamber is from photon interactions in the gas itself. This violates one of the main assumptions of Bragg–Gray cavity theory and thus they concluded: “Bragg–Gray cavity theory can be safely applied to megavoltage photon radiation dosimetry but not to low- (up to 100 keV) and medium-energy (100–300 keV) photon beams.” At the 300 keV energy typical in an ^{192}Ir source, they found a 3% breakdown in the assumptions, with

roughly a 30% breakdown at 100 keV. If the breakdown in the assumptions led to a reduction in the accuracy of the theory, then a primary standard for ^{192}Ir based on a cavity ion chamber would be inappropriate.

The main purpose of the present work is to establish the accuracy of Spencer–Attix cavity theory as applied with a graphite-walled ion chamber for photon energies from 20 to 1300 keV, with particular emphasis on photon energies applicable to ^{192}Ir . For this purpose we study in detail the response of: (a) the cylindrical NRC ion chamber which is used as Canada’s primary standard for air kerma in a ^{60}Co beam,³ (b) the pancake chamber used by the BIPM for the same purpose,⁸ and (c) the spherical chambers used as primary standards by NIST.⁹

The approach used is a pragmatic one rather than a theoretical one. We calculate the ion chamber’s response using Monte Carlo techniques and we also calculate the response predicted by Spencer–Attix cavity theory using the standard, state-of-the-art calculations of stopping-power ratios and other correction factors. We then investigate any discrepancies.

To accomplish this goal requires accurate calculation of ion chamber response using Monte Carlo techniques. Up until recently, the calculation of ion chamber response was one of the most difficult tasks for electron-photon Monte Carlo codes. Despite a long history of such calculations,^{10–18} the

overall accuracy was still limited to about 1%.¹⁹ However, there has been significant progress in this area and with the development of the EGSnrc Monte Carlo code²⁰ it is now possible to calculate absolute ion chamber response (normalized against its own cross sections, i.e., independent of the uncertainties in the cross sections) to within 0.1% for ⁶⁰Co photons²¹ and with a similar accuracy for photons at energies down to 10 keV.²² Using the techniques described below, this development allows us to verify directly the accuracy of cavity theory with a similar accuracy.

In doing this study we started with the assumption that the small amount of nongraphite material in the chamber had no effect. This assumption is used by all standards laboratories that we are aware of. However, we have found that it has a significant effect in the case of the NRC chamber and hence we have also studied the size of this correction.

II. THEORY

The Spencer–Attix schematization of Bragg–Gray cavity theory is based, amongst other things, on the assumption that the dose to the gas in the cavity is caused by electrons generated in the walls of the cavity. All photons are assumed to pass through the cavity. This is stated in the following two Bragg–Gray conditions,¹ where a gas layer g is placed in a material w .

- The thickness of the g -layer is assumed to be so small in comparison with the range of charged particles striking it that its presence does not perturb the charged-particle field.
- The absorbed dose in the cavity is assumed to be deposited by charged particles crossing it.

Spencer and Attix²³ showed that the effect of secondary electrons needs to be considered, an effect which the Bragg–Gray theory does not take into account. Later Nahum²⁴ reworked Spencer–Attix theory to consider energy dissipation by the electron track-ends explicitly. Nahum’s formulation of the Spencer–Attix theory gives a ratio of the doses in media w and g of

$$\frac{D_w}{D_g} = \left(\frac{\bar{L}}{\rho} \right)_g^w = \frac{\int_{\Delta}^{E_{\max}} \Phi_E \left(\frac{L(\Delta)}{\rho} \right)_w dE + \Phi_E(\Delta) \left(\frac{S(\Delta)}{\rho} \right)_w \Delta}{\int_{\Delta}^{E_{\max}} \Phi_E \left(\frac{L(\Delta)}{\rho} \right)_g dE + \Phi_E(\Delta) \left(\frac{S(\Delta)}{\rho} \right)_g \Delta}, \quad (1)$$

where Φ_E is the fluence of particles with energy E , $(S(\Delta)/\rho)$ is the unrestricted mass collision stopping-power evaluated at energy $E = \Delta$, and Δ is the lowest energy for which secondary electrons are considered part of the electron spectrum.²⁴ All secondaries with energy below Δ are considered absorbed on the spot and are accounted for in the restricted stopping-power, $(L(\Delta)/\rho)$.

Using the Spencer–Attix relationship for a parallel beam of photons, the air kerma, K_{air} , at the location of the center of an ion chamber when the chamber is not there is given by²⁵

$$K_{\text{air}} = D_{\text{gas}} \left(\frac{\bar{L}}{\rho} \right)_{\text{gas}}^{\text{wall}} \left(\frac{\bar{\mu}_{\text{en}}}{\rho} \right)_{\text{wall}}^{\text{air}} \frac{1}{(1 - \bar{g}_{\text{wall}})} K K_{SA}, \quad (2)$$

where $(\bar{\mu}_{\text{en}}/\rho)_{\text{wall}}^{\text{air}}$ is the average ratio of mass energy-absorption coefficients in the air and the wall material; \bar{g} is the average fraction of the electron’s energy lost via radiative processes, i.e., to bremsstrahlung production,²⁶ and the Spencer–Attix correction factor, K_{SA} , is introduced here to account for any departure from Spencer–Attix cavity theory as it is normally applied. In the Monte Carlo simulation of this case, the correction factor K reduces to K_{wall} , a correction factor for attenuation and scattering in the chamber wall, since no humidity correction is required for the dry air used in the simulations, and we use a parallel photon beam, i.e., there is no correction for axial nonuniformity of the beam. Since we can calculate $K_{\text{air}}(1 - \bar{g})$ from the incident photon spectrum and the mass energy-absorption coefficients for air [see Eq. (4) below], and except for K_{SA} , we can calculate all the quantities on the right-hand side in the equation using Monte Carlo techniques, thus we can use this equation to deduce K_{SA} . The factor K_{SA} will account for any corrections such as fluence corrections^{27,28} or a breakdown in the calculation of stopping-power ratios and is given by

$$K_{SA} = \frac{K_{\text{air}}(1 - \bar{g}_{\text{wall}})}{D_{\text{gas}} \left(\frac{\bar{L}}{\rho} \right)_{\text{gas}}^{\text{wall}} \left(\frac{\bar{\mu}_{\text{en}}}{\rho} \right)_{\text{wall}}^{\text{air}} K_{\text{wall}}}. \quad (3)$$

In this work we explicitly calculate K_{SA} using the EGSnrc Monte Carlo system, which has been shown to calculate ion chamber response with an accuracy at the 0.1% level.^{21,22} Accuracy in this context means “relative to the given cross sections,” and hence for Eq. (3) to be meaningful it is critical to use a self-consistent set of cross-section data for all calculated quantities.

III. CALCULATIONS AND RESULTS

The newly developed and substantially improved version of the Monte Carlo code EGS4, i.e., EGSnrc,²⁰ is used to calculate the various factors in Eq. (3) to obtain the values of K_{SA} . The dose to the air in the cavity, D_{gas} , and the correction factor for scattering and attenuation in the wall, K_{wall} , are calculated using the NRC user codes CAVRZnrc (for cylindrical geometry) and CAVSPHnrc (for spherical geometry). These codes are based on the CAVRZ code originally developed by Bielajew *et al.*¹¹ which was updated recently to work with EGSnrc²⁹ and from which several bugs were removed. These codes have been used extensively³⁰ and shown to give the same results as CAVRZ working with EGS4 for

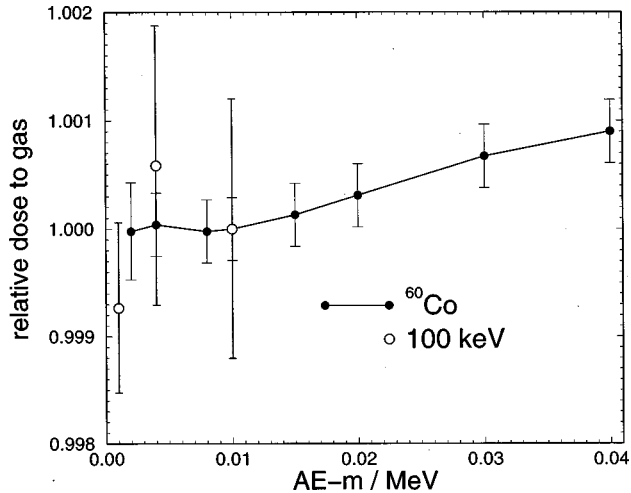


FIG. 1. Variation in the dose to the gas as a function of the threshold for creation of secondary electrons (AE) which was equal to $ECUT$ in all calculations. The filled symbols are for an incident beam of ^{60}Co photons and the open symbols are for incident 100 keV photons (which require much longer calculations). All values are normalized to the dose in each case for the standard value of $AE-m$ of 10 keV, where m is the rest mass of the electron.

corrections such as at K_{wall} , although the overall calculated response differs because it uses the EGSnrc Monte Carlo simulation system.^{20,21,31} The calculation of K_{wall} with Monte Carlo techniques has been extensively studied^{12,30,32} and is thought to be accurate to better than 0.1%.

In all cases the EGSnrc system is used without binding, relaxation, or spin effects taken into account. Since this study is independent of the cross sections used, in principle it doesn't matter if we include these effects or not. Moreover, for the calculations being done here, we find that turning on or off any of these effects has no effect on the calculated values of D_{gas} at the 0.1% level at 100 keV and 1.25 MeV.

Electrons are followed down to 521 keV (total) and photons down to 1 keV (i.e., $AE=ECUT=0.521$ and $AP=PCUT=0.001$). As shown in Fig. 1, for the chambers under investigation here, we have found that using lower values of $ECUT$ led to the same values of D_{gas} . We have found that the value of $ECUT$ needed to obtain a stable estimate of the dose to the gas depends very much on the dimensions of the cavity involved and smaller cavities require lower values of $ECUT$.

For all graphite densities used, the ICRU Report 37 density correction for graphite with density 1.70 g cm^{-3} is applied.^{33,34} The conclusions of this study are independent of the details of which density effect is used. The photon spectra used for ^{192}Ir and ^{60}Co sources are based on Monte Carlo simulations of the relevant sources.^{5,35}

A. Ion chambers

Three types of graphite ionization chambers are modeled in the calculations in order to examine the issues in a wide variety of geometric shapes. These ion chambers are currently used as standards for air kerma in ^{60}Co beams at the National Research Council of Canada (NRC), at the Bureau

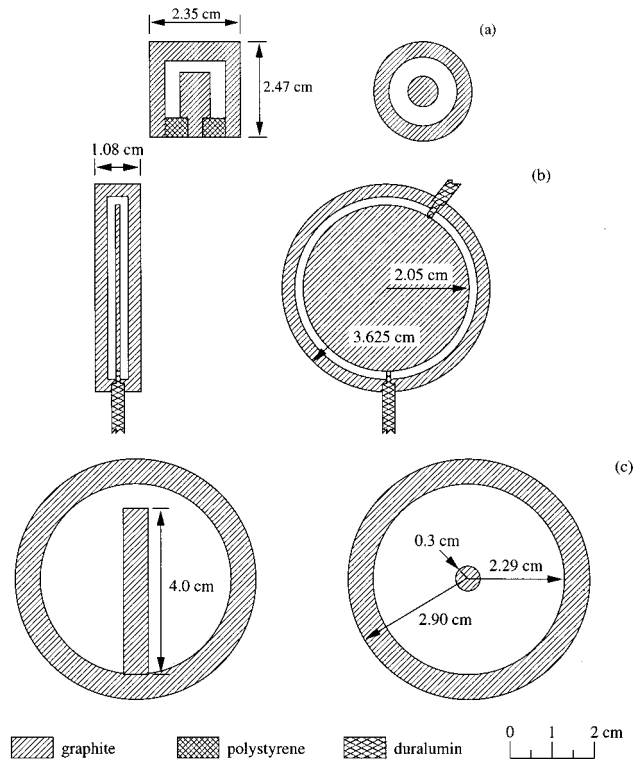


FIG. 2. Cross sections of the models of the cylindrical NRC ion chamber (a), the parallel plate BIPM ion chamber (b), and the 50 cm^3 spherical NIST ion chamber (c). In the calculation of the departure from Spencer–Attix theory, the nongraphite materials in the chambers are replaced with graphite.

International des Poids et Mesures (BIPM, France), and at the National Institute for Standards and Technology (NIST), respectively.

The NRC (3C) ion chamber³ was built by W. H. Henry at NRC and has been used as the Canadian ^{60}Co air-kerma standard since the late 1950s. A small mass of air is surrounded by enough material to ensure full buildup. The material of the wall and central electrode are graphite with a density of 1.66 g cm^{-3} and one end cap is made of polystyrene. Figure 2(a) shows the cross section of the NRC ion chamber which has cylindrical geometry. The chamber is modeled as shown and any effects from stem scatter are accounted for elsewhere. Basic cavity theory applies to a cavity in one material only. For the calculations related to the accuracy of Spencer–Attix cavity theory, the polystyrene in the NRC chamber is replaced with graphite in the calculations. A correction for materials different from the wall in the ion chamber, K_{comp} , is discussed in Sec. III H.

The BIPM ion chamber⁸ has a flat cylindrical shape and is made of graphite with a circular collecting plate in the middle of the cavity as shown in Fig. 2(b). The collector plate is held by two small rods of Duralumin (aluminum alloy). The density of the graphite used for this chamber is 1.84 g cm^{-3} . Monte Carlo calculations are performed for a model of the BIPM chamber with no Duralumin holders and for a model with the area of the holders exposed to the air modeled as two rings in the chamber (to maintain cylindrical

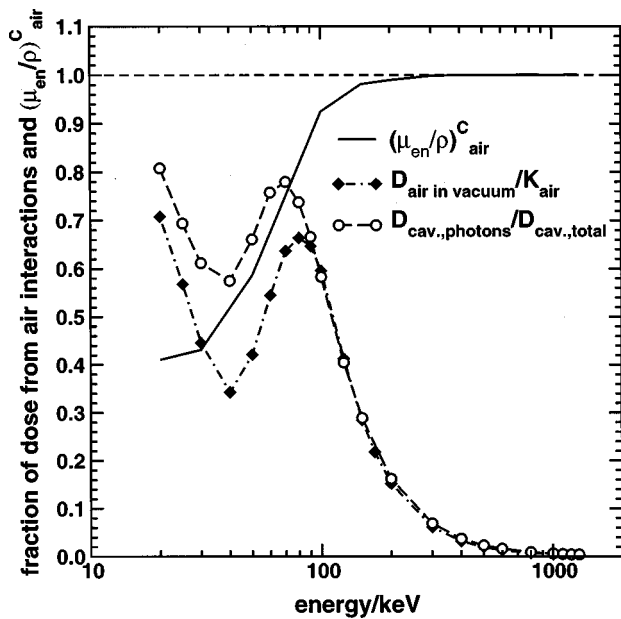


FIG. 3. Fraction of dose to the air in the cavity from photon interactions in the air for the NRC chamber is shown together with the ratio of mass energy-absorption coefficients graphite to air. The curve with filled diamonds is the ratio of the dose in an air cavity (same dimensions as the cavity of the NRC ion chamber) in vacuum to the air kerma for the actual photon beam. The curve with open circles is the ratio of two simulations which include the walls of the chamber in the calculation, but in one case electron transport in the walls is turned off so that only the dose from photon interactions in the cavity is included. The difference in the two ratios is caused by the contribution of photons scattered in the walls.

geometry) to estimate the effect of the holders on the chamber response, i.e., K_{comp} .

The NIST ion chambers⁹ used as primary standards are spherical with volumes of 1, 10, 30, and 50 cm³. Only the chambers with wall thicknesses of approximately 4 mm are modeled, and for these chambers the collector electrode is not included in the calculation, since the user code CAVSPHnrc only allows spherical geometries and the collector electrode is a cylinder. The density of graphite for the NIST chambers is 1.73 g cm⁻³. An example of one of these spherical ion chambers is shown in Fig. 2(c).

Detailed dimensions of the ion chambers are available elsewhere and are not critical to the issues under discussion here.^{3,8,9}

B. Photon interactions in cavity

The breakdown of the assumption that photons do not deposit energy in the cavity is studied for an air cylinder placed in a vacuum. The absorbed dose to the air is calculated using CAVRZnrc for monoenergetic, parallel photon beams incident on the side of the cylinder. The air cavity has a diameter of 1.58 cm and is 1.61 cm long, similar to the actual dimensions of the air cavity in the NRC chamber when ignoring the electrode. The ratio of absorbed dose from photon interactions in the air divided by the air kerma is shown in Fig. 3. This represents the extreme nonequilibrium situation, since no photons are scattered and attenuated in the wall, and no electrons are starting or reflected from the walls.

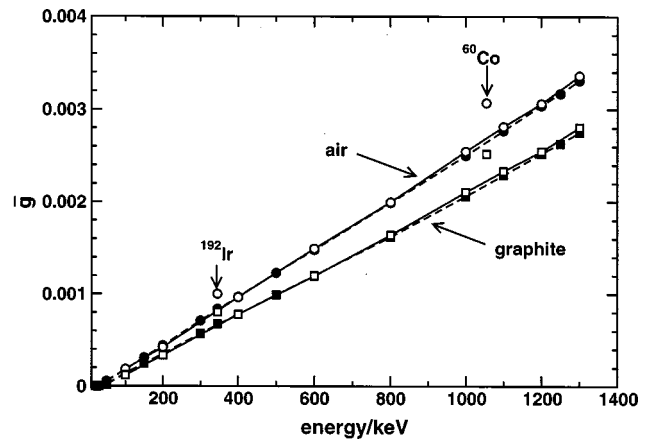


FIG. 4. Values of \bar{g} for air and graphite. The closed symbols represent the values from Boutillon (Ref. 26) and the open symbols are values calculated from the cross-section data set used in the present Monte Carlo calculations (for $E \geq 100$ keV). The new ^{60}Co values and the ^{192}Ir values are plotted at the mean energy of the spectrum used (Refs. 5 and 35). The statistical uncertainties are typically 0.5% but the overall uncertainty is determined by the 5% uncertainty in the underlying radiative stopping power from ICRU Report 37 (Ref. 33).

This result is similar to that of Ma and Nahum,⁷ taking the larger diameter and length of the air cavity into account.

The absorbed dose due to photon interactions in the air cavity when it is part of the graphite chamber is calculated by simulating the entire chamber and discarding all electrons set in motion in the graphite wall. Only photons which interact in the air contribute to the dose. These can be primary photons which are attenuated by the walls or photons scattered in the wall. There is a slight underestimate of this dose because electrons generated in the air do not scatter back from the walls in the calculations. The ratio of dose in the cavity from photon interactions there to the total dose in the cavity is shown as a function of photon energy in Fig. 3. For the actual cavity, the fraction of the dose due to photon interactions in the cavity at 300 keV is 7%, and at 100 keV the fraction is 60%.

C. Data on \bar{g}

The fraction of the electron's energy lost via radiative processes, \bar{g} , is calculated in a Monte Carlo calculation using the PEGS4 data sets with the ICRU radiative cross sections.^{33,36} EGSnrc includes a correction³¹ to the EGS4 bremsstrahlung sampling routines which causes a 2% or 3% change in the calculated value of \bar{g} in this case compared to EGS4 (but which had no effect for more typical cases for electrons with energies \gg AP). A small user code is used which scores all the energy radiated by electrons slowing down after being created by photons interacting in an infinite medium and also scores all the energy transferred by these photons to electrons. \bar{g} is just the ratio of these two quantities. Figure 4 shows the values of \bar{g} over the energy range from 100 to 1300 keV compared to the values taken from Boutillon²⁶ which are based on a simpler calculation using the ICRU Report 37 radiative yields.³³ The present values are about 2% higher than the previous values near ^{60}Co en-

ergies. This is consistent with the results of Seltzer,³⁷ who found that in this energy range the radiative yields calculated using Monte Carlo simulations are 3% higher than those calculated using CSDA models as used in ICRU Report 37. The values for ⁶⁰Co from the current calculations are plotted at the mean energy for the spectrum used, viz. 1055 keV to emphasize that one cannot interpolate for the value of a spectrum based on using a mean photon energy.

These comparisons to previous work are to emphasize the accuracy of the code and its internal consistency. The overall uncertainty on the calculated value of \bar{g} is dominated by the uncertainty on the bremsstrahlung cross section which is estimated as 5% in ICRU 37 (pg. 48).

D. Mass energy-absorption coefficients and air kerma

In the calculation of K_{SA} it is important to ensure consistent use of photon cross sections. Therefore the mass energy-absorption coefficients for air and for graphite are derived using the cross sections in EGSnrc via the user-code DOSRZnrc. The dose to a 2 μm thick air or graphite slab of “infinite” radius is calculated for a monoenergetic parallel photon beam which is forced to interact in the slab. There is no electron transport and thus no radiation loss due to bremsstrahlung. Hence we are calculating the kerma, K , when we calculate the dose. The mass energy-absorption coefficients in air and graphite are calculated from

$$K_Z = \Psi \left(\frac{\mu_{\text{en}}}{\rho} \right)_{E,Z} \frac{1}{(1 - \bar{g}_{E,Z})} \quad [\text{Gy}], \quad (4)$$

where Ψ is the energy fluence and E and Z denote the photon energy and the effective atomic number, respectively.²⁵

The graphite to air ratios of mass energy-absorption coefficients calculated in this way are shown in Fig. 3. Above 300 keV the mass energy-absorption coefficient is the same for air and graphite to within 0.1%. These values above 300 keV, which are calculated with the PEGS4 data sets, are within 0.4% of the latest values by Hubbell and Seltzer,³⁸ although the disagreement reaches 3% for energies below 100 keV.

Given the mass-energy absorption coefficients and \bar{g} , it is a straightforward extension of Eq. (4) to calculate the air kerma in a photon spectrum. Alternatively, one can calculate the kerma directly as described above using a Monte Carlo calculation. We get the same answer both ways.

E. Stopping-power ratios

The restricted stopping-power ratios graphite to air are calculated using the NRC user code SPRRZnrc,^{29,39} which makes use of the restricted stopping powers based on ICRU Report 37.^{33,34} The density of graphite used in the calculation of stopping-power ratios is 1.66 g cm⁻³, since that is the real bulk density of the NRC chamber, and the density correction used is for graphite with a density of 1.70 g cm⁻³, since that is one of the two values for which the density effect was calculated by the ICRU. The standard cutoff energy for the calculation of the stopping-power ratios is the same as for all

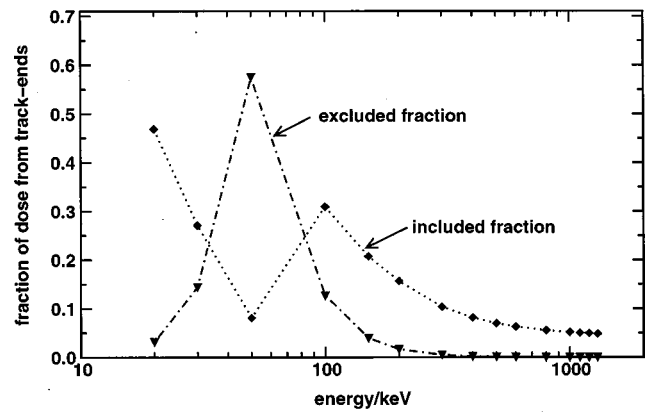


Fig. 5. Fraction of dose from track-ends included and excluded in the track-end term when calculating stopping-power ratios for monoenergetic photons incident on a graphite mini-phantom. The dose fraction from excluded track-ends is less than 2% at energies higher than 200 keV.

other Monte Carlo calculated values in this work, namely 521 or $\Delta = 10$ keV. This value is used for consistency with the other calculated values and because it is the widely used value in radiation dosimetry.^{40,41} However, as will be discussed below, this value requires more careful consideration for primary standards of air kerma.^{8,9,42}

We study two methods of calculating the stopping-power ratio,

- (1) The stopping-power ratios are calculated for the actual electron spectrum in the mini-phantom or wall material at the point of measurement (this is the commonly used method);
- (2) the stopping-power ratios are calculated for the electron spectrum at the same point but created only by the unattenuated primary photons—a geometry independent calculation.

1. Method 1

A parallel photon beam is incident on the side of a cylinder with dimensions similar to the NRC chamber but consisting entirely of the material for which the stopping-power ratio is calculated, with a scoring volume of the same dimensions as the ion chamber’s air cavity. The stopping-power ratios are calculated with track-ends using the scoring-on-the-fly techniques described earlier.³⁹ The track-ends include both electrons slowing down and crossing the Δ value (“included fraction”), and electrons created (by photon interactions) with energies below Δ (“excluded fraction”). Electrons created with energies below Δ are not included in the calculated stopping-power ratio, whereas those slowing down past Δ are properly included. Figure 5 shows the fraction of the dose from included and excluded track-ends as a function of photon energy. The complex shapes reflect the change in mean electron energy as photoelectric and Compton scattering dominate at different energies. Note that for 1.25 MeV photons if one ignores the “included” components of track-ends when calculating the stopping-power ra-

tio (a 5% dose component), the effect on the stopping-power ratio is at most a few tenths of a percent. However, it is not clear how to interpret the excluded fraction.

If one takes the Spencer–Attix formulation at face value and considers the track ends as part of the in-phantom electron spectrum, then these electrons must somehow be taken into account. Given the large contribution to the dose from the excluded component of the track-ends at low energies, it is hard to estimate the effect on the stopping-power ratios of these excluded track-ends. Presumably it is negligible above 200 keV where this component represents at most 2% of the dose and the mass energy-absorption coefficients for graphite and air are so similar. However, it could become significant at lower energies.

Alternatively, one can ask, what do these electrons correspond to when we consider the cavity situation? They can only correspond to photon interactions in the cavity which create these electrons with energies below Δ since phantom generated electrons created below Δ cannot get into the cavity region. From this perspective we are free to exclude them from the calculation of the stopping-power ratio since Spencer–Attix cavity theory assumes such interactions do not occur. However, once one adopts this point of view, viz that the calculations somehow include interactions in the cavity, then, one must ask how do we exclude the effects of electrons generated in the cavity with energies greater than Δ ?

With either of the above approaches, Fig. 5 implies that there are problems calculating stopping-power ratios for photon energies of around 100 keV or lower. The issue of proper calculation of stopping-power ratios will require further research to sort out all the subtleties, but in the meantime we are adopting a pragmatic approach to assessing the size of the problem. As we show below, the factor K_{SA} becomes significant for photon energies of 100 keV and below and hence the need for calculated stopping-power ratios at these energies for practical applications is negligible.

2. Method 2

The first method is appropriate for stopping-power ratios needed at depth in a phantom, since the effects of attenuation and scatter in the phantom are needed. However, for an ion chamber free in air, the theory of ion chamber response calls for stopping-power ratios for the unattenuated primary photon beam.^{27,28} To calculate these stopping-power ratios, an option has been added to SPRRZnrc in which photons are regenerated after interactions and secondary photons are discarded. With this calculation there is no attenuation in the wall and the calculation of stopping-power ratio is independent of the geometry of the ion chamber. Figure 6 presents the graphite to air stopping-power ratio for monoenergetic photon beams with energies from 20 to 1300 keV and for the spectra for ^{192}Ir and ^{60}Co . Note that the issue regarding the excluded fraction affects stopping-power ratios calculated with method 2 as well as method 1.

Figure 7 shows the ratio of the stopping-power ratios calculated using methods 1 and 2. Method 1 includes the effects

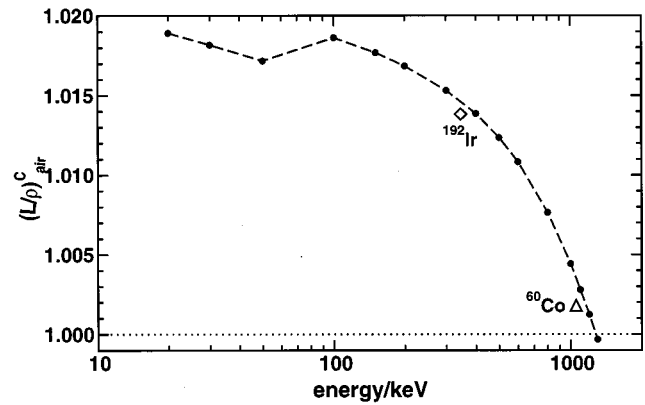


Fig. 6. Stopping-power ratios calculated with the user-code SPRRZnrc and the geometry independent method 2 as described in Sec. III E. The graphite density effect used is for 1.70 g cm^{-3} .

of lower-energy scattered photons and thus calculates a slightly higher stopping-power ratio, although the difference is not significant.

F. Departure from Spencer–Attix cavity theory

The calculation of all the terms on the right-hand side of Eq. (3) has been described and from these the values of K_{SA} can be calculated and are shown as a function of photon energy in Figs. 8 and 9 for the homogeneous NRC and BIPM ion chambers, respectively. The K_{SA} corrections for incident beams from an encapsulated ^{192}Ir HDR brachytherapy source (microSelectron) with an average energy of 345 keV,⁶ and from ^{137}Cs and ^{60}Co sources are shown as well. It is seen that a straightforward application of Spencer–Attix cavity theory is valid within 0.2% down to a photon energy of 500 keV for the NRC chamber and down to a photon energy of 600 keV for the BIPM chamber. At 100 keV, the deviation of K_{SA}

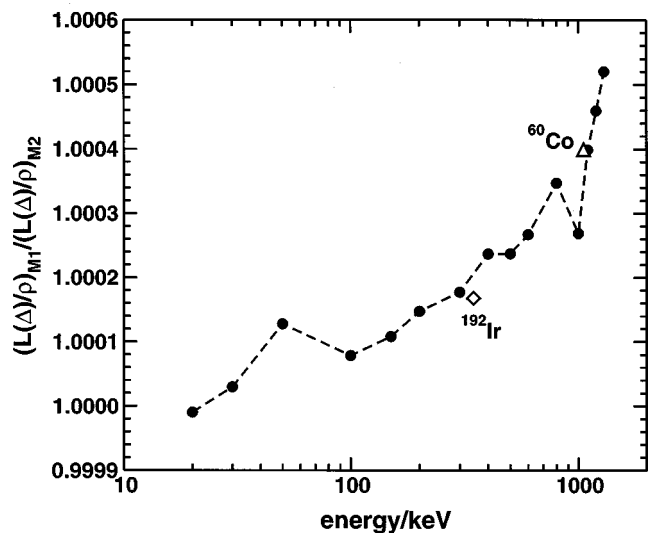


Fig. 7. Ratio of Spencer–Attix graphite to air stopping-power ratios calculated using method 1 (including scatter and attenuation in the wall) and method 2 (geometry independent with no scatter) as described in Sec. III E. The value of Δ for the calculations is 10 keV.

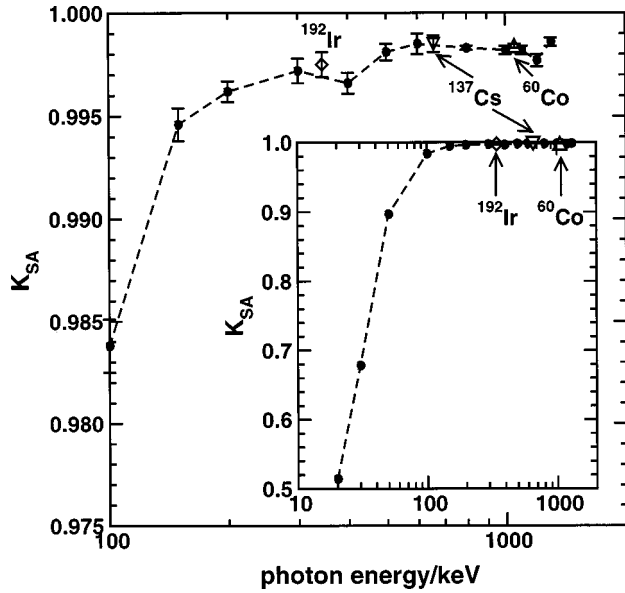


FIG. 8. Values of the Spencer–Attix correction factors, K_{SA} , for the NRC cylindrical ion chamber made entirely of graphite as a function of energy for monoenergetic photon beams and for three spectra. All calculations are done with $\Delta = 10$ keV and shown with a statistical uncertainty of 1 standard deviation. The inset shows the agreement for the full interval from 20 to 1300 keV.

from unity is only about 2% for the NRC chamber, despite the fact that over 60% of the ion chamber response is coming from photon interactions in the gas as shown by Fig. 3 and this violates one of the Bragg–Gray conditions.

For the NRC chamber, Fig. 8 shows that straightforward

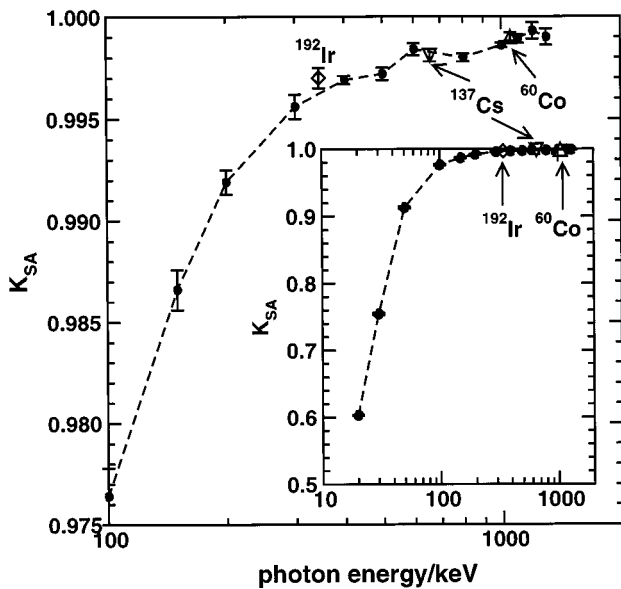


FIG. 9. Values of the Spencer–Attix correction factors, K_{SA} , for the BIPM pancake ion chamber made entirely of graphite as a function of energy for monoenergetic photon beams and for three spectra. All calculations are done with $\Delta = 10$ keV and shown with a statistical uncertainty of 1 standard deviation. The inset shows the agreement for the full interval from 20 to 1300 keV.

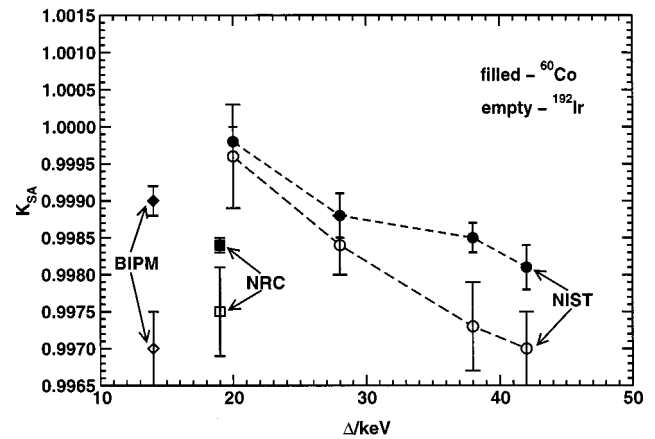


FIG. 10. Values of K_{SA} for ^{192}Ir and ^{60}Co beams, calculated when using the standard $\Delta = 10$ keV cutoff to calculate stopping-power ratios for the NIST spherical ion chambers, and the NRC and BIPM ion chambers. They are plotted as a function of the value of Δ implied by the simple 4 V/A chord length prescription for each chamber as discussed in the text. At ^{60}Co and ^{192}Ir the departure from Spencer–Attix theory using $\Delta = 10$ keV for all types of ion chambers is less than 0.2% and 0.3%, respectively.

application of Spencer–Attix cavity theory is only 0.3% less accurate at 200 keV than it is at ^{60}Co and about 0.1% less accurate at ^{192}Ir than at ^{60}Co . For the BIPM chamber the breakdown is somewhat worse relative to ^{60}Co but the breakdown for ^{192}Ir is still very small (0.2%) as seen in Fig. 9.

In Fig. 10 the agreement with Spencer–Attix cavity theory for ^{60}Co and ^{192}Ir beams is compared for the NRC, the BIPM and the NIST ion chambers. For all chambers the agreement at ^{60}Co is within 0.2% and at ^{192}Ir within 0.3%. These results are obtained using $\Delta = 10$ keV but have been plotted vs the value of Δ appropriate to their geometries (see next section).

G. Variation of stopping-power ratios with Δ

As mentioned above, the Δ value, i.e., the cutoff (kinetic) energy in the Monte Carlo calculation of stopping-power ratio, is traditionally taken as 10 keV for dosimetry protocols.^{40,41,43} However, for primary standards of air kerma it is usually varied according to the size of the cavity.^{8,9,42} The exact definition of Δ within Spencer–Attix theory is rather vague, but it is related to the lowest energy of electrons, which can just cross the cavity. This can be related to the mean chord length across the cavity, which for a convex cavity in an isotropic field is given by¹ $l = 4V/A$, where V is the volume of the air in the cavity, and A its surface area. Taking Δ to be the electron energy for which the residual CSDA range is just the mean chord length implies Δ values for the NRC and BIPM chambers of 19 keV (530 keV total) and 14 keV (525 keV total), respectively, and for the NIST chambers Δ varies from 20 to 42 keV. Figure 11 shows the normalized stopping-power ratio graphite to air at ^{60}Co and at ^{192}Ir as a function of Δ . At ^{60}Co there is a variation of 0.17% between the stopping-power ratios calculated with $\Delta = 10$ and $\Delta = 42$ keV. The values of K_{SA} calculated using Δ values based on the mean chord length are shown in Fig. 12.

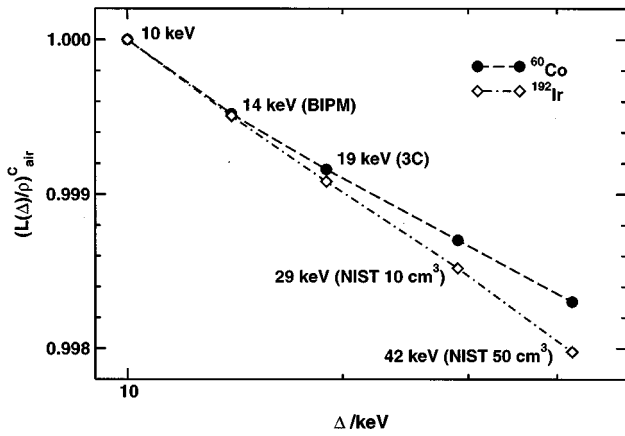


FIG. 11. Normalized stopping-power ratio graphite to air at ⁶⁰Co and at ¹⁹²Ir as a function of Δ, the cutoff energy for the Monte Carlo calculation. Δ is derived from the mean chord length. Note that the x-axis is logarithmic. The stopping-power ratios are normalized to 1.000 at 10 keV, where the values are 1.0018 and 1.0138 for ⁶⁰Co and ¹⁹²Ir, respectively.

Using a Δ value based on the mean chord length brings all calculated K_{SA} values for ⁶⁰Co within 0.1% of unity and for ¹⁹²Ir, within about 0.2% of unity. The choice of Δ value is thus very important for the calculation of the agreement with Spencer–Attix cavity theory.

H. Composite wall materials

Practical ion chambers do not consist of graphite alone, since the collector electrode must be held in place and insulated by another material. As seen in Fig. 2 the insulator in the NRC chamber is a ring of polystyrene, and in the BIPM chamber there are holders made of Duralumin (aluminum alloy). To take this into account one introduces a correction factor K_{comp} into Eq. (2) as another of the K factors.²⁵ The correction is not required for the investigation of the agreement with Spencer–Attix cavity theory, but for obtaining the dose or air kerma from a measurement, this correction, in principle, should be applied, although usually it does not appear to be considered.^{8,9,42}

Using Monte Carlo simulations the value of K_{comp} is calculated as the ratio of the calculated dose to the air (corrected for attenuation and scatter) for a model with only graphite

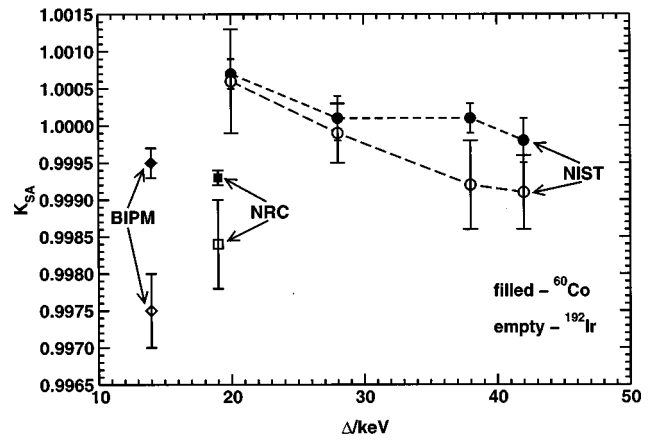


FIG. 12. Values of K_{SA} for ¹⁹²Ir and ⁶⁰Co beams, calculated when stopping-power ratios are calculated using values of Δ implied by the simple 4V/A chord length prescription for each chamber as discussed in the text. They are plotted as a function of the value of Δ used in each case. At ⁶⁰Co and ¹⁹²Ir the departure from Spencer–Attix theory for the NIST chambers is largest for the 50 cm³ chamber (Δ = 42 keV) but still less than 0.1%.

walls and end caps to the calculated dose for a model with graphite walls and a polystyrene insulator (for the NRC chamber) or a model with holders of Duralumin (for the BIPM chamber).

$$K_{comp,MC} = \frac{(D_{gas} K_{wall})_{graphite}}{(D_{gas} K_{wall})_{polystyrene \text{ or } Duralumin}} \tag{5}$$

The Monte Carlo calculated K_{comp} values for the NRC chamber as a function of photon energy are shown in Fig. 13.

To estimate the K_{comp} value through Monte Carlo calculations for the BIPM chamber the two holders for the collector plate are modeled as two rings, one on the side of the collector and one behind the collector with outer radius equal to that of the collector. Care is taken to have the same mass and the same area of Duralumin exposed to the air as in the real BIPM ion chamber. Modeling the holders correctly is not possible with the user code CAVRZnrc, since it models cylindrical geometries only.

An analytical expression of the effect of composite walls is generally used for calculating the influence of a buildup cap made of a different material than the chamber wall,²⁵

$$K_{comp,ana} = \frac{1}{\left(\frac{\bar{L}}{\rho}\right)_{air}^{wall} \left(\frac{\bar{\mu}_{en}}{\rho}\right)_{wall}^{air} \left[\alpha \left(\frac{\bar{L}}{\rho}\right)_{wall}^{air} \left(\frac{\bar{\mu}_{en}}{\rho}\right)_{air}^{wall} + (1 - \alpha) \left(\frac{\bar{L}}{\rho}\right)_{cap}^{air} \left(\frac{\bar{\mu}_{en}}{\rho}\right)_{air}^{cap} \right]}, \tag{6}$$

where α is the fraction of the ionization in the cavity due to electrons originating in the wall material and (1 - α) is the fraction from the buildup cap. In the present case, we make the rough approximation that this expression applies for the effect of different materials near the cavity, e.g., polystyrene

or Duralumin. For the analytical calculation of K_{comp} , α must be estimated. For the NRC chamber the fraction of the dose to the air in the cavity originating from the graphite is calculated using the user code DOSRZnrc. For the BIPM chamber the α value is estimated from the surface area of Duralu-

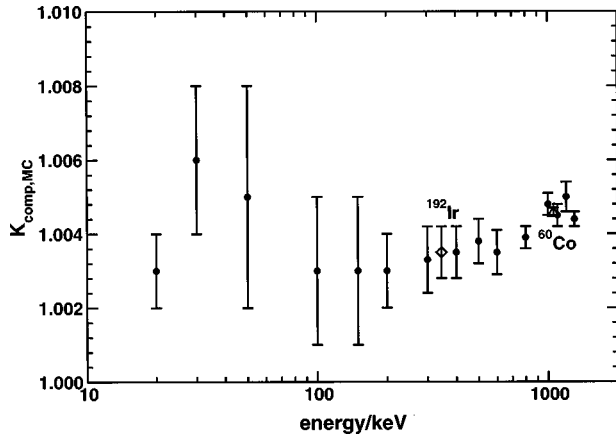


FIG. 13. Monte Carlo calculated correction factors for nongraphite materials in the NRC 3C ion chamber, $K_{\text{comp,MC}}$ as a function of incident photon energy. The average value of $K_{\text{comp,MC}}$ is 1.004 ± 0.001 (1 standard deviation).

min compared to that of graphite. This latter value is only a very crude estimate! A worst case scenario for the BIPM chamber is obtained by fitting the mass of Duralumin into the two rings and covering the actual area of graphite in the Monte Carlo model. This means that much more Duralumin surface is exposed to the air and $K_{\text{comp,MC}}$ is 0.9970 ± 0.0003 .

Table I shows the results of calculations of K_{comp} from Eqs. (5) and (6) for the NRC chamber and for the BIPM chamber with polystyrene and Duralumin, respectively, as part of the chamber material. The results of calculations using the simple analytical expression agree well with the Monte Carlo calculated values, and K_{comp} indicates either a decrease ($K_{\text{comp}} > 1$) or an increase ($K_{\text{comp}} < 1$) in the dose to the cavity compared to the dose in a homogeneous chamber, depending on what material is used in addition to the graphite. The values calculated are surprisingly large given that standards laboratories have not traditionally considered this correction factor of 0.4% for the NRC chamber and of -0.07% for the BIPM chamber.

IV. CONCLUSIONS

The calculations demonstrate that the standard formulation of Spencer-Attix cavity theory with $\Delta = 10$ keV has an accuracy, when using graphite-walled ion chambers for cali-

TABLE I. Correction for composite materials in the NRC and BIPM ion chambers in a ^{60}Co beam. $K_{\text{comp,ana}}$ and $K_{\text{comp,MC}}$ are calculated from Eqs. (5) and (6), respectively. The analytically calculated K_{comp} for the NRC chamber is based on a Monte Carlo calculation (with the user code DOS-RZnrc) of the fraction of dose, α , in the cavity due to particles originating in the graphite wall. The Monte Carlo calculated values are given with 1 standard deviation uncertainties in brackets. $K_{\text{comp,ana}}$ for the BIPM chamber is not given with an uncertainty since the areas of graphite and Duralumin are “exact” (same as used in the Monte Carlo simulation).

Chamber	$K_{\text{comp,ana}}$	$K_{\text{comp,MC}}$
NRC	1.0041(5)	1.0038(2)
BIPM	0.9990	0.9993(2)

brating ^{192}Ir sources, which is comparable to that for ^{60}Co sources. For 200 keV photons, the theory is within 0.3% of the accuracy at ^{60}Co energies despite the demonstrated breakdown of the assumption that there are no photon interactions in the cavity. This conclusion must not be generalized to chambers of other wall materials, and is not expected to hold in general since we have only shown the theory to be accurate, which is different from being correct!

We have shown that the standard formulation of Spencer-Attix cavity theory used in dosimetry protocols (i.e., $\Delta = 10$ keV) breaks down in ^{60}Co beams by amounts ranging from 0.02% to 0.2%. This breakdown can be characterized by the mean chord length of the electrons crossing the cavity of the ion chambers involved and hence Δ (see Fig. 10). However, we have also shown that this is mostly explained by the inadequacy of using $\Delta = 10$ keV in the standard formulation instead of using a Δ value more closely associated with the mean chord length (see Fig. 11). Many standards laboratories already take this into account.^{8,9,42}

Calculating the stopping-power ratio for the electron spectrum created by the unattenuated primary photon interactions in the graphite (geometry independent) gives a slightly smaller value—up to 0.04% at ^{60}Co —than calculating the value for the actual electrons in the cavity as seen in Fig. 7. Although the difference is not large, it is the former values which are required by the underlying theory.^{27,28}

Although the main emphasis in this study has been lower energy photons, the results for ^{60}Co beams demonstrate that Spencer-Attix theory, as normally applied by standards laboratories, is accurate, at least within the calculational uncertainty of EGSnrc of 0.1% or so. Note that this assessment of the cavity theory can be made at this high level of accuracy because the uncertainty in cross-section data drops out of consideration.

In addition, we have shown that a correction for composite wall material, e.g., insulators and holders, should be included in the correction factors applied to a measurement. This factor is found to be 0.999 (BIPM) and 1.004 (NRC) for two of the chamber types studied, which leads to a 0.5% difference in the measured responses of air kerma if no such correction is applied. This is of significance in a primary standard of air kerma.

Viewed overall, these calculations demonstrate a remarkable consistency of cavity theory and high-quality Monte Carlo calculations. However, it must be recognized that if we use these results to justify the application of Spencer-Attix cavity theory for ^{192}Ir beams, this amounts to making the Monte Carlo calculations an intrinsic part of the standard.

ACKNOWLEDGMENTS

This work was supported by the National Institutes of Health through Research Grant No. 1 R01 CA66852. We wish to thank our colleague, Alan Nahum, for perceptive comments on the manuscript.

^aElectronic mail: dave.rogers@nrc.ca

¹F. H. Attix, *Introduction to Radiological Physics and Radiation Dosimetry* (Wiley, New York, 1986).

- ²M.-T. Niatel, T. P. Loftus, and W. Oetzmann, "Comparison of exposure standards for ^{60}Co gamma rays," *Metrologia* **11**, 17–23 (1975).
- ³K. R. Shortt and C. K. Ross, "The Canadian ^{60}Co exposure standard," National Research Council of Canada Report PIRS-0052 (1986).
- ⁴T. P. Loftus, "Standardization of iridium-192 gamma-ray sources in terms of exposure," *J. Res. Natl. Bur. Stand.* **85**, 19–25 (1980).
- ⁵J. Borg and D. W. O. Rogers, "Spectra and air-kerma strength for encapsulated ^{192}Ir sources," *Med. Phys.* **26**, 2441–2444 (1999).
- ⁶J. Borg and D. W. O. Rogers, "Monte Carlo calculations of photon spectra in air from ^{192}Ir sources," NRC Report PIRS-629r (1998). (See <http://www.irs.inms.nrc.ca/inms/irs/papers/PIRS629r/pirs629r.html>) (1998).
- ⁷C. M. Ma and A. E. Nahum, "Bragg-Gray theory and ion chamber dosimetry for photon beams," *Phys. Med. Biol.* **36**, 413–428 (1991).
- ⁸M. Boutillon and M.-T. Niatel, "A study of a graphite chamber for absolute exposure measurements of ^{60}Co gamma rays," *Metrologia* **9**, 139–146 (1973).
- ⁹T. P. Loftus and J. T. Weaver, "Standardization of ^{60}Co and ^{137}Cs gamma-ray beams in terms of exposure," *J. Res. Natl. Bur. Stand., Sect. A* **78A**, 465–476 (1974).
- ¹⁰J. E. Bond, R. Nath, and R. J. Schulz, "Monte Carlo calculation of the wall correction factors for ionization chambers and A_{eq} for ^{60}Co γ rays," *Med. Phys.* **5**, 422–425 (1978).
- ¹¹A. F. Bielajew, D. W. O. Rogers, and A. E. Nahum, "Monte Carlo simulation of ion chamber response to ^{60}Co —Resolution of anomalies associated with interfaces," *Phys. Med. Biol.* **30**, 419–428 (1985).
- ¹²D. W. O. Rogers, A. F. Bielajew, and A. E. Nahum, "Ion chamber response and A_{wall} , correction factors in a ^{60}Co beam by Monte Carlo simulation," *Phys. Med. Biol.* **30**, 429–443 (1985).
- ¹³A. C. McEwan and V. G. Smyth, "A Monte Carlo technique for evaluation of cavity ionization chamber correction factors," NRL Report Number 1983/7, Christchurch, New Zealand (1983).
- ¹⁴A. C. McEwan and V. G. Smyth, "Comments on calculated response and wall correction factors for ionization chambers exposed to ^{60}Co gamma-rays," *Med. Phys.* **11**, 216–218 (1984).
- ¹⁵V. G. Smyth, "Interface effects in the Monte Carlo simulation of electron tracks," *Med. Phys.* **13**, 196–200 (1986).
- ¹⁶V. G. Smyth and A. C. McEwan, "Interface artefacts in Monte Carlo calculations," *Phys. Med. Biol.* **31**, 299–301 (1986).
- ¹⁷A. F. Bielajew and D. W. O. Rogers, "Interface artefacts in Monte Carlo calculations," *Phys. Med. Biol.* **31**, 301–302 (1986).
- ¹⁸B. J. Foote and V. G. Smyth, "The modeling of electron multiple-scattering in EGS4/PRESTA and its effect on ionization-chamber response," *Nucl. Instrum. Methods Phys. Res. B* **100**, 22–30 (1995).
- ¹⁹D. W. O. Rogers, "How accurately can EGS4/PRESTA calculate ion chamber response?," *Med. Phys.* **20**, 319–323 (1993).
- ²⁰I. Kawrakow, "Accurate condensed history Monte Carlo simulation of electron transport. I. EGSnrc, the new EGS4 version," *Med. Phys.* **27**, 485–498 (2000).
- ²¹I. Kawrakow, "Accurate condensed history Monte Carlo simulation of electron transport. II. Application to ion chamber response simulations," *Med. Phys.* **27**, 499–513 (2000).
- ²²J. P. Seuntjens, I. Kawrakow, and D. W. O. Rogers, "Accuracy tests of the new EGSnrc Monte Carlo system in the simulation of ion chamber response in low energy photon beams," *Med. Phys.* (abstract) **26**, 1121 (1999).
- ²³L. V. Spencer and F. H. Attix, "A theory of cavity ionization," *Radiat. Res.* **3**, 239–254 (1955).
- ²⁴A. E. Nahum, "Water/air stopping-power ratios for megavoltage photon and electron beams," *Phys. Med. Biol.* **23**, 24–38 (1978).
- ²⁵D. W. O. Rogers, "Fundamentals of high energy x-ray and electron dosimetry protocols," in *Advances in Radiation Oncology Physics*, Medical Physics Monograph 19, edited by J. Purdy (AAPM, New York, 1992), pp. 181–223.
- ²⁶M. Boutillon, " \bar{g} values from Berger and Seltzer tables (1982)," BIPM document CCEMRI(I)/85-18 (1985).
- ²⁷A. F. Bielajew, "Ionization cavity theory: A formal derivation of perturbation factors for thick-walled ion chambers in photon beams," *Phys. Med. Biol.* **31**, 161–170 (1986).
- ²⁸A. F. Bielajew, "An analytic theory of the point-source non-uniformity correction factor for thick-walled ionisation chambers in photon beams," *Phys. Med. Biol.* **35**, 517–538 (1990).
- ²⁹D. W. O. Rogers, I. Kawrakow, J. P. Seuntjens, and B. R. B. Walters, "NRC User Codes for EGSnrc," Technical Report PIRS-702, National Research Council of Canada, Ottawa, Canada (2000).
- ³⁰D. W. O. Rogers and J. Treurniet, "Monte Carlo calculated wall and axial non-uniformity corrections for primary standards of air kerma," NRC Report PIRS-663, NRC, Ottawa (1999).
- ³¹I. Kawrakow and D. W. O. Rogers, "The EGSnrc Code System: Monte Carlo simulation of electron and photon transport," Technical Report PIRS-701, National Research Council of Canada, Ottawa, Canada (2000).
- ³²D. W. O. Rogers and A. F. Bielajew, "Wall attenuation and scatter corrections for ion chambers: Measurements versus calculations," *Phys. Med. Biol.* **35**, 1065–1078 (1990).
- ³³ICRU, "Stopping powers for electrons and positrons," ICRU Report 37, ICRU, Washington D.C. (1984).
- ³⁴S. Duane, A. F. Bielajew, and D. W. O. Rogers, "Use of ICRU-37/NBS collision stopping powers in the EGS4 system," NRCC Report PIRS-0173, Ottawa, March (1989).
- ³⁵D. W. O. Rogers, G. M. Ewart, A. F. Bielajew, and G. van Dyk, "Calculation of electron contamination in a ^{60}Co therapy beam," in *Proceedings of the IAEA International Symposium on Dosimetry in Radiotherapy* (IAEA, Vienna, 1988), Vol. 1, pp. 303–312.
- ³⁶D. W. O. Rogers, S. Duane, A. F. Bielajew, and W. R. Nelson, "Use of ICRU-37/NBS radiative stopping powers in the EGS4 system," National Research Council of Canada Report PIRS-0177 (1989).
- ³⁷S. M. Seltzer, "Calculation of photon mass energy-transfer and mass energy-absorption coefficients (dosimetry application)," *Radiat. Res.* **136**, 147–170 (1993).
- ³⁸J. H. Hubbell and S. M. Seltzer, "Tables of x-ray mass attenuation coefficients and mass energy-absorption coefficients 1 keV to 20 MeV for elements Z=1 to 92 and 48 additional substances of dosimetric interest," Technical Report NISTIR 5632, NIST, Gaithersburg, MD (1995).
- ³⁹A. Kosunen and D. W. O. Rogers, "Beam quality specification for photon beam dosimetry," *Med. Phys.* **20**, 1181–1188 (1993).
- ⁴⁰AAPM TG-21, "A protocol for the determination of absorbed dose from high-energy photon and electron beams," *Med. Phys.* **10**, 741–771 (1983).
- ⁴¹IAEA, *Absorbed Dose Determination in Photon and Electron Beams; An International Code of Practice*, Technical Report Series (IAEA, Vienna, 1987), Vol. 277.
- ⁴²M. P. T. R. F. Laitano, "The primary exposure standard for ^{60}Co gamma radiation: Characteristics and measurements procedures," ENEA Report RT/PROT(83)28 (1983).
- ⁴³P. R. Almond, P. J. Biggs, B. M. Coursey, W. F. Hanson, M. S. Huq, R. Nath, and D. W. O. Rogers, "AAPM's TG-51 protocol for clinical reference dosimetry of high-energy photon and electron beams," *Med. Phys.* **26**, 1847–1870 (1999).